

An orientation-field model for polycrystalline solidification with a singular coupling between order and orientation

Hervé Henry, Jesper Mellenthin, and Mathis Plapp

Physique de la Matière Condensée, École Polytechnique, CNRS, 91128 Palaiseau, France

(Dated: July 30, 2012)

The solidification of polycrystalline materials can be modelled by orientation-field models, which are formulated in terms of two continuous fields: a phase field that describes the thermodynamic state and an orientation field that indicates the local direction of the crystallographic axes. The free-energy functionals of existing models generally contain a term proportional to the modulus of the orientation gradient, which complicates their mathematical analysis and induces artificial long-range interactions between grain boundaries. We present an alternative model, in which only the square of the orientation gradient appears, but in which the phase and orientation fields are coupled by a singular function that diverges in the solid phase. We show that this model exhibits stable grain boundaries whose interactions decay exponentially with their distance. Furthermore, we demonstrate that the anisotropy of the surface energy can be included while preserving the variational structure of the model. Illustrative numerical simulations of two-dimensional examples are also presented.

I. INTRODUCTION

In polycrystalline materials that consist of multiple crystalline grains of the same thermodynamic phase, the grain size and texture of the material largely determine mechanical properties such as toughness and yield stress. Therefore, a large effort has been devoted to understanding the relation between the processing conditions during solidification and subsequent ageing of a material and the resulting grain structure. From a fundamental viewpoint, this is an example of self-organization [1]: a complex structure emerges from a structureless initial state (the liquid), and the resulting network of grain boundaries evolves with time and coarsens [2, 3].

Despite a large body of work, many questions regarding this self-organization process remain open. As often in such complex problems, a comparison between experiments and numerical modeling could be highly useful. Therefore, it is desirable to develop quantitative modeling tools for the solidification and evolution of polycrystalline materials. Among the many modelling approaches, the phase-field method has rapidly gained in popularity in recent years due to its versatility and robustness. For recent reviews on its applications in materials science, see Refs. [4–6].

Numerous phase-field models for the description of polycrystalline solidification and grain growth have already been developed. They can be grouped in two categories. In the so-called multi-phase-field approach [7–11], each grain is described by an individual phase field. The grain boundary energies are determined by the coupling between the phase fields. Despite the necessity to handle a large number of phase fields, this approach can be made quite efficient from a numerical point of view [10, 12]. Nevertheless, it suffers from the fact that for each simulation the coupling coefficients between the phase fields need to be computed (and stored) in order to reproduce the proper grain boundary energies [11]. Moreover, since the crystalline orientation in each grain is fixed, phenom-

ena such as grain rotation and plastic deformation cannot easily be described. Finally, from a fundamental point of view, a large number of fields certainly does not constitute the most “economic” description of a polycrystalline structure, since the state of matter in any space point can be specified by a set of a few variables, such as the degree of order and the local lattice orientation.

As a consequence of the latter consideration, alternative models have been developed that use a single phase field coupled to an orientation field [13–18]. The phase field describes the local thermodynamic state – either solid ($\phi = 1$) or liquid ($\phi = 0$) – and the orientation field is used to describe the local orientation of the crystallographic axes in the solid with respect to some fixed reference system. In two dimensions, the orientation field is simply an angle $\theta(\mathbf{x}, t)$, while in three dimension a more complex formalism is needed [19, 20]. In this framework, a grain boundary is a diffuse but localized region in space between two regions of the same thermodynamic state (both are solid) but different crystalline orientations. The change of the crystalline orientation is concentrated in the grain boundary where the phase field is no longer equal to 1.

While this kind of description is appealing, it turns out that the construction of a viable model is far from simple because of the need to obtain localized grain boundaries. Let us consider the two-dimensional (2D) case with a scalar angle field and try to construct a free energy functional that leads to localized solid-liquid interfaces and grain boundaries. For the solid-liquid interfaces, this is straightforward: since there are two privileged and distinct thermodynamic states (solid and liquid), diffuse interfaces arise from the free energy balance between a double-well potential and a square-gradient term for the phase field. In the case of grain boundaries, matters are not so simple. Indeed, there is no privileged angle and the free energy must be rotationally invariant. Therefore, a potential that depends on the angle is forbidden, and only terms that contain spatial derivatives of θ can be

used in the free energy. Then, in order to model localized grain boundaries, at a first glance it seems sufficient to introduce a term that couples the energy cost of angular variations to the local value of the phase field and induces a sufficiently high energy penalty for angle variations in the solid.

However, a simple scaling argument, reviewed in detail below, shows that localized grain boundaries cannot be obtained by a straightforward coupling of a square-gradient term in θ to the phase field. In fact, such a model is equivalent to the usual thermodynamic description of nematic liquid crystals [21], in which indeed no “grain boundaries” (localized changes in the director field) exist. The solution proposed in the previous orientation-field models is to include an additional term proportional to $|\nabla\theta|$ in the free energy. Localized grain boundaries then arise from the balance between this term and the square gradient in θ . While this approach yields localized grain boundaries, it also has several problems. First, from a fundamental viewpoint it seems difficult to justify such a form in the spirit of a Landau expansion. Second, the functional derivative of this non-analytic term leads to a singular diffusion equation for θ and to non-local interactions between grain boundaries [22]. The latter effect can be removed by a proper regularization [16], but this introduces additional parameters into the model.

Here, we propose an alternative approach. Our model contains only a square gradient term in θ , but relies on the use of a singular coupling function between orientation and phase field to make the energy cost of angular variations in the solid effectively infinite. Similar ideas were proposed some years ago by Lusk [23], but were to our best knowledge not pursued any further until now. The interesting point about this approach is that the equations for the equilibrium grain boundaries and solid-liquid interfaces are ordinary (non-singular) differential equations that can be analyzed using standard mathematical tools and concepts from dynamical systems theory. Furthermore, it turns out that the dynamical equations for the angle field show the proper behavior, that is, no long-range interactions between grain boundaries arise. Therefore, we believe that this approach can be a useful alternative to existing orientation-field models.

The remainder of the paper is organized as follows. In Sec. II, we first outline the model (for isotropic interfaces) and then show how to determine a suitable coupling function between phase and orientation fields that yields localized grain boundaries. Furthermore, we discuss in detail the properties of these grain boundary solutions. In Sec. III, we then extend the model to include interfacial anisotropy, and present numerical tests both in one and two dimensions to show that the model has the desired properties. Perspectives for future work are discussed in Sec. IV.

II. MODEL

A. General remarks and outline

We consider a two-dimensional system in which the crystal orientation can be described by a single angle field $\theta(\mathbf{x}, t)$; the local state of the system is described by a phase field $\phi(\mathbf{x}, t)$. We start from a free energy of the form

$$F = \int d\mathbf{x} \left[\frac{D}{2} (\nabla\phi)^2 + HV(\phi, T) + Kg(\phi)(\nabla\theta)^2 \right], \quad (1)$$

where D , H et K are constants. Furthermore, the dimensionless function $V(\phi, T)$ is a temperature-dependent double-well potential with minima at $\phi = 1$ (solid) and $\phi = 0$ (liquid), and g is a function that tends to zero for $\phi \rightarrow 0$. For simplicity, we have neglected crystalline anisotropy for the moment; its inclusion will be discussed below.

Let us first consider a coupling function $g(\phi)$ that takes a finite value $g(1)$ in the solid. The scaling argument which proves that there are no localized grain boundary solutions in this case is as follows. In the absence of anisotropy, the grain boundary solution must depend only on the total angle change (misorientation) $\Delta\theta$ between the two grains. For a solid of size L with a homogeneous continuous orientation variation between $\Delta\theta/2$ and $-\Delta\theta/2$, the energy cost (with respect to a state of constant θ) is $g(1)KL(\Delta\theta/L)^2$ which decreases monotonously with growing L and tends to zero when $L \rightarrow \infty$. In contrast, any localized grain boundary solution has an energy that is independent of the system size (and includes the energy cost for the variation of the phase field). For sufficiently large L , the uniform angle variation has therefore always lower energy than a localized grain boundary. More precisely, whereas grain boundaries can be stable in finite systems depending on the values of L and $g(1)$, an isolated grain boundary in an infinite system is always unstable. This scaling argument also clarifies why a term of the form $|\nabla\theta|$ cures this problem: with such a term, the energy of a homogeneous variation of the angle is independent of the system size and can be made larger than the energy of a localized solution by a proper choice of coupling functions and parameters.

Here, we propose an alternative approach to achieve the same goal. Since the above argument holds only for a finite value of $g(1)$, a possible way out is to use a *singular* coupling function $g(\phi)$ that tends to infinity when $\phi \rightarrow 1$. The rationale for this idea is that in a crystalline material any continuous variation of the local orientation implies an elastic or plastic strain, which has a high energy cost. We will show below that we can indeed choose a singular coupling function that leads to grain boundaries with the desired properties. This function cannot be explicitly linked to microscopic physics or an elastic model; our approach is therefore essentially phenomenological.

For the sake of definiteness, we use a coupling function of the form

$$g(\phi) = \frac{f(\phi)}{(1-\phi)^\alpha}, \quad (2)$$

where α is some positive real exponent and f is a polynomial in ϕ which satisfies $f(0) = 0$ and $f(1) = 1$.

It is useful for the following developments to non-dimensionalize the free energy functional and the involved length scales. The functional has three parameters: D and K have dimensions of energy per unit length, and H sets a free energy (density) scale for the (dimensionless) double-well potential $V(\phi, T)$. Dividing the whole functional by H , we obtain

$$F = \int d\mathbf{x} \left[\frac{W_\phi^2}{2} (\nabla\phi)^2 + V(\phi, T) + W_\theta^2 g(\phi) (\nabla\theta)^2 \right], \quad (3)$$

where $W_\phi = \sqrt{D/H}$ and $W_\theta = \sqrt{K/H}$ are the characteristic length scales associated with solid-liquid interfaces and grain boundaries, respectively. Scaling all lengths with W_ϕ and defining $\mu = W_\theta/W_\phi$, we finally obtain

$$F = \int d\mathbf{x} \left[\frac{1}{2} (\nabla\phi)^2 + V(\phi, T) + \mu^2 g(\phi) (\nabla\theta)^2 \right]. \quad (4)$$

In the following, we consider the case $\mu = 1$ that can be obtained by a proper rescaling of θ by μ . It should be pointed out that this is also the best case for a useful model since then the characteristic thickness of solid-liquid interfaces and grain boundaries are comparable.

The equations of motion for the two fields are obtained by the standard variational procedure [13–18],

$$P(\phi, \nabla\theta) \tau_\phi \partial_t \phi = -\frac{\delta F}{\delta \phi}, \quad (5)$$

$$Q(\phi, \nabla\theta) \tau_\theta \partial_t \theta = -\frac{\delta F}{\delta \theta}, \quad (6)$$

where τ_ϕ and τ_θ are relaxation times, and $P(\phi, \nabla\theta)$ and $Q(\phi, \nabla\theta)$ are (dimensionless) mobility functions.

For the solidification of a pure substance, the motion of solid-liquid interfaces is linked to heat transport by the Stefan condition (the latent heat released or consumed at moving interfaces must be transported by the local diffusion currents). The model therefore has to be completed by an equation for the temperature field. We define a dimensionless temperature u by

$$u(\mathbf{x}, t) = \frac{T(\mathbf{x}, t) - T_m}{L/c}, \quad (7)$$

where T_m , L , and c are the melting temperature, the latent heat of fusion, and the specific heat, respectively. The field u obeys the same equation as in the standard phase-field model,

$$\partial_t u = D_{\text{th}} \nabla^2 u + \partial_t \phi, \quad (8)$$

with D_{th} the thermal diffusion coefficient.

It turns out that in order to obtain a model with the desired properties, a certain number of conditions on the exponent α , the polynomial f and the double-well potential V have to be satisfied that are linked in a sometimes subtle way to the internal structure of the grain boundary. In order to facilitate the understanding of the following developments, it seems useful at this point to state a summary of these results, while the details of the arguments will be given below. The main points are the following.

1. Localized grain boundary solutions which smoothly connect to an infinite bulk solid on both sides can exist only for $\alpha \geq 2$.
2. For a fixed total misorientation $\Delta\theta$ and increasing system size L , the energy cost of a uniformly strained solid tends to zero for $\alpha < 2$ and to infinity for $\alpha > 2$. Together with condition 1, this yields that the only reasonable value for α is 2.
3. The requirement that the angle variation is strongly concentrated in the center of the grain boundary imposes that the first term appearing in the polynomial f is of order ϕ^3 .
4. A uniformly strained solid must be stable against the spontaneous formation of grain boundaries. This imposes the relation $ab - d > 0$, where $a = V'''(1)/2$, $d = -V'''(1)/6$, and $b = -f'(1)$, and primes denote a derivative with respect to ϕ .
5. For $\alpha = 2$, the competition between the gradient terms of the phase field and the orientation field makes it impossible to obtain stable grain boundaries with misorientations smaller than a critical misorientation $\Delta\theta_m$. The magnitude of $\Delta\theta_m$ is controlled by the same combination of parameters that appears in condition 4, $ab - d$.

In particular, the last point has implications for the choice of the double-well potential V . In the standard phase-field model for solidification, this potential is $V(\phi) = \phi^2(1-\phi)^2 + u\lambda(10\phi^3 - 15\phi^4 + 6\phi^5)$, where λ is a dimensionless coupling parameter. For this potential, the second derivatives with respect to the phase field, $V''(\phi, T)$, are independent of temperature in both wells ($\phi = 0$ and $\phi = 1$); however, the third derivatives depend on the temperature. For our model, this would yield a temperature-dependent minimal grain boundary misorientation. We prefer to use a potential where, in addition to the above properties, the third derivative of V in the solid well is kept constant. Furthermore, since for the calculations of the grain boundary energy the solid state is the reference state, we wish to keep the energy of the solid potential well independent of temperature and equal to zero, whereas the height of the liquid potential minimum varies with temperature.

A set of model functions which satisfies all the above requirements and conditions is

$$g = \frac{7\phi^3 - 6\phi^4}{(1 - \phi)^2} \quad (9)$$

$$V = \phi^2(1 - \phi)^2 - u\lambda(1 - 20\phi^3 + 45\phi^4 - 36\phi^5 + 10\phi^6) \quad (10)$$

These functions will be used in the numerical examples given below. In the following, we will first give the details of the arguments that lead to the restrictions on these functions, and then discuss their consequences on the structure of the grain boundary solutions, in particular concerning the dependence of these solutions on temperature.

B. Construction of the coupling function: the details

Our model should have one-dimensional grain boundaries as equilibrium solutions. In the framework used here, a grain boundary is a localized interface (region where ϕ is smaller than 1) between two solids (semi-infinite regions where $\phi = 1$) with different crystal orientations. Therefore, we are looking for appropriate stationary solution of Eqs. (5) and (6). The calculation of the functional derivative yields

$$0 = \partial_x(g(\phi)\partial_x\theta), \quad (11)$$

$$0 = -V'(\phi, T) + \partial_{xx}\phi - g'(\phi)(\partial_x\theta)^2. \quad (12)$$

From Eq. (11), we obtain that at equilibrium

$$g(\phi)\partial_x\theta = C, \quad (13)$$

where C is a constant to be determined later. Inserting this expression into Eq. (12) yields

$$\partial_{xx}\phi = V'(\phi, T) + g'(\phi)\frac{C^2}{g(\phi)^2}, \quad (14)$$

$$= -\frac{d}{d\phi} \left[-V(\phi, T) + \frac{C^2}{g(\phi)} \right]. \quad (15)$$

The second equality puts this equation in a form suitable for the use of the well-known analogy with a mechanical system: replacing x by t and ϕ by y , one obtains the equation of a particle with coordinate y moving in a potential

$$V_{\text{eff}}(y) = -V(y, T) + \frac{C^2}{g(y)} \quad (16)$$

(see Fig. 1 (a)). The grain boundary solution corresponds then to the trajectory of a particle that starts with zero velocity at the unstable equilibrium point $y = 1$, (the point A in Fig. 1(a), which corresponds to the solid state) and reaches the turning point $y = y_0$ (the point B in

Fig. 1 (a)), in an infinite time and comes back. The infinite duration of the trajectory corresponds to the condition that the limit of ϕ in the bulk is $\phi = 1$ (solid) on both sides of the grain boundary. This leads to the requirement that $\phi = 1$ must be an equilibrium point of V_{eff} , i.e.

$$\left. \frac{dV_{\text{eff}}}{d\phi} \right|_{\phi=1} = -V'(1) - C^2(1 - \phi)^{\alpha-1} \frac{\alpha f + (1 - \phi)f'}{f^2} \Big|_{\phi=1} = 0, \quad (17)$$

where we have supposed $\alpha > 1$ for V_{eff} to be differentiable in $\phi = 1$. In addition, $\phi = 1$ must correspond to an unstable equilibrium point of V_{eff} , that is, the second derivative of the effective potential must be negative for $\phi \rightarrow 1$. A simple argument helps to determine the sign of the second derivative. Since the double-well potential $V(\phi, T)$ has a minimum at $\phi = 1$, we can expand it around this value as $V(\phi, T) \approx V(1, T) + V''(1, T)(1 - \phi)^2/2$. Then the effective potential becomes

$$V_{\text{eff}} = -V(1, T) + (1 - \phi)^2 \left(-V''(1, T)/2 + C^2 \frac{(1 - \phi)^{\alpha-2}}{f(\phi)} \right). \quad (18)$$

From this expression, it is clear that the sign of V''_{eff} at $\phi = 1$ is determined by the sign of the function $s(\phi) = (-V''(1, T)/2 + C^2(1 - \phi)^{\alpha-2}/f(\phi))$ at $\phi = 1$. If $\alpha - 2 > 0$, the second term in this function tends to zero for $\phi \rightarrow 1$, whereas $-V''(1, T)$ is finite and negative. Therefore, $s(1)$ is negative. In contrast, if $\alpha - 2 < 0$, the second term becomes dominant for $\phi \rightarrow 1$, and s is positive. If $\alpha = 2$, $s = (-V''(1, T)/2 + C^2/f(\phi))$. In this case, since $f(1) = 1$, s changes sign when C^2 crosses $-V''(1, T)/2$.

In summary, the fact that 1 must be an unstable equilibrium point of V_{eff} imposes to choose $\alpha \geq 2$. We proceed by showing that the study of the homogeneous solid solution imposes $\alpha = 2$. To do this, we consider a long homogeneous solid of length L where θ is varying from $\Delta\theta/2$ to $-\Delta\theta/2$ with constant gradient $\partial_x\theta = \Delta\theta/L$. The scaling argument outlined above shows that a regular coupling function yields an energy cost of such a homogeneous solution that goes to zero when $L \rightarrow \infty$ at constant $\Delta\theta$; we would hence like to construct a model in which this is not the case. Qualitatively, it is easy to see why this can be achieved with a singular coupling function. As long as $\partial_x\theta$ is different from zero, the singularity forbids the phase field to take the value $\phi = 1$ corresponding to the solid, since this would imply an infinite energy cost. However, when $\partial_x\theta$ decreases, the phase field can get closer and closer to $\phi = 1$. Therefore, whereas $(\partial_x\theta)^2$ decreases, the value of $g(\phi)$ increases, which can be used to tune the dependence of the total energy on the system size. The requirement that the energy must remain finite (it should not go to zero, but not tend to infinity either when $L \rightarrow \infty$) then fixes the exponent α .

Let us now make this argument quantitative. Since we consider a weakly distorted solid, we can assume that ϕ is close to 1. Let $\delta = 1 - \phi$ where ϕ is the (constant) value of the phase field. Since ϕ is constant, the gradient in the phase field does not contribute to the energy of

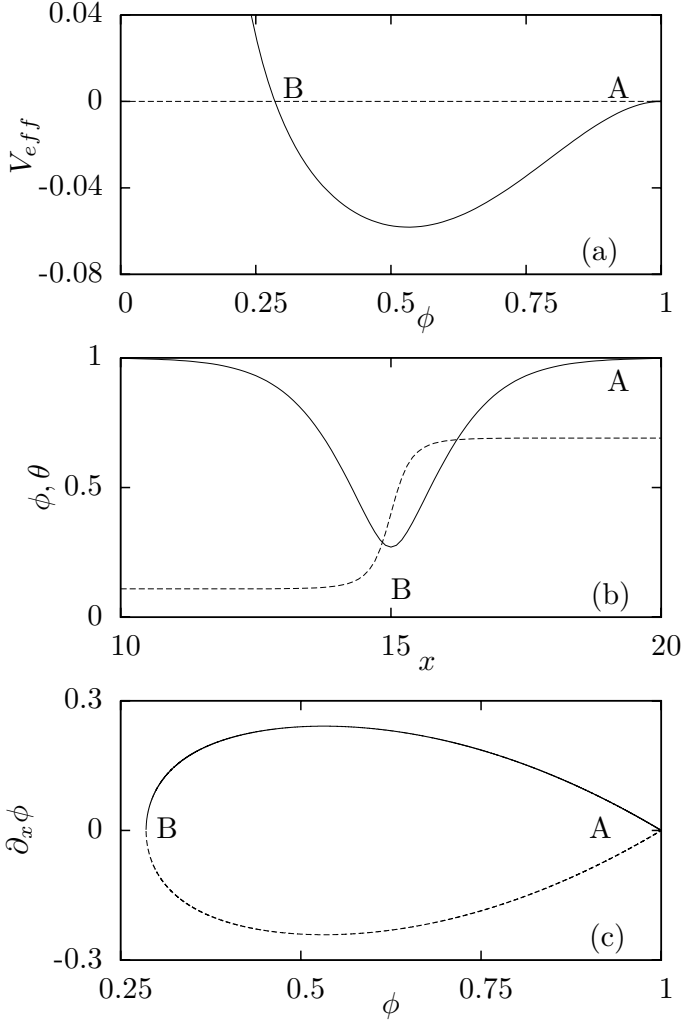


FIG. 1. (a) Schematic drawing of a typical effective potential V_{eff} . The starting point of the trajectory corresponding to $\phi = 1$ is A, the turning point is B. In both A and B, $\partial_x \phi = 0$. (b) Typical profiles of ϕ (solid line) and θ (dashed line) through a grain boundary. A corresponds to the limit $\phi \rightarrow 1$ and $x \rightarrow \pm\infty$. (c) Grain boundary solution, plotted in the phase space spanned by ϕ and $\partial_x \phi$.

this state. Keeping the dominant term in δ in the two remaining terms of the free energy functional, we obtain for the energy E of the state with homogeneous angle variation,

$$E = L \left[\frac{\delta^2}{2} V''(1) + \frac{(\partial_x \theta)^2}{\delta^\alpha} \right]. \quad (19)$$

Minimization of this expression with respect to δ yields

$$\delta = \left(\frac{\alpha (\partial_x \theta)^2}{V''(1)} \right)^{1/(\alpha+2)}. \quad (20)$$

Using this expression in Eq. (19), we find

$$E = L \left[Q \left(\frac{\Delta \theta}{L} \right)^{4/(\alpha+2)} \right], \quad (21)$$

where $Q = [V''(1)/2][\alpha/V''(1)]^{2/(\alpha+2)} + [V''(1)/\alpha]^{\alpha/(\alpha+2)}$ is positive. The only possible value for α that yields a finite energy in the limit of large L is $\alpha = 2$. With this choice, the energy of a large system with constant angle variation is proportional to $\Delta \theta$.

The requirement that this homogeneous solution must be stable yields another condition. To understand its origin, consider the curve $E(L)$. If this curve is concave, there is an instability that is analogous to spinodal decomposition: at fixed total $\Delta \theta$, it is more advantageous for the system to concentrate the distortion in one or several regions because this lowers the total energy; in other words, there would be spontaneous formation of grain boundaries. To prevent this, the curve $E(L)$ should be convex at least for low values of the distortion (weakly strained solids), which implies that it has to tend to the limit value from above. To find the corresponding mathematical condition, the expansion in δ has to be pushed to higher order, where the energy writes (for $\alpha = 2$)

$$E = L \left[a\delta^2 + d\delta^3 + \left(\frac{\Delta \theta}{L} \right)^2 \frac{1 + b\delta + c\delta^2}{\delta^\alpha} \right] \quad (22)$$

where $a = V''(1)/2$, $d = -V'''(1)/6$, $b = -f'(1)$, and $c = f''(1)/2$. Using the fact that $(\Delta \theta/L)^2 \sim \delta^{\alpha+2}$ according to Eq. (20), it is straightforward to show that the requirement of $E(L)$ to be a decreasing function of L for $L \rightarrow \infty$ implies

$$ab + d > 0. \quad (23)$$

To finish with the study of the homogeneous solution, we find it useful to present some numerical results using the complete model. The computation of the energy as a function of L for a fixed value of $\Delta \theta$ gives the expected result that the energy density depends only on the value of $\Delta \theta/L$: $E/L = \mathcal{E}(\Delta \theta/L)$. The function $\mathcal{E}(\Delta \theta/L)$ is plotted in figure 2 (a). It is interesting to note that in this case, the value of dE/dL is a function of $\Delta \theta/L$ only. These results also show that, up to a rescaling of the energy E and the length L , all the curves of the energy as a function of L collapse onto a single master curve which is plotted in figure 2 (b). This curve presents a maximum, the position of which is given by the solution of the equation

$$\mathcal{E}(\Delta \theta/L) = \left(\frac{\Delta \theta}{L} \right) \mathcal{E}'(\Delta \theta/L). \quad (24)$$

C. Grain boundary solutions

We now turn to a more complete description of the grain boundary equilibrium solutions for $\alpha \geq 2$. They can be easily computed using the mechanical analog outlined above. For a given value of C , one first computes the value of ϕ_0 corresponding to the turning point (B in

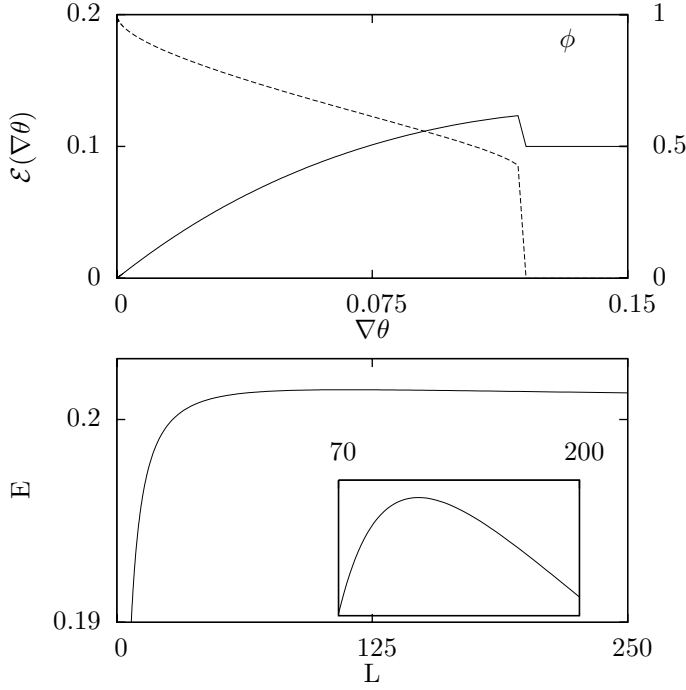


FIG. 2. (a) solid line: $E/L = \mathcal{E}(\Delta\theta)$ as a function of $\nabla\theta = \Delta\theta/L$, dashed line: ϕ as a function of $\Delta\theta/L$. For values of $|\nabla\theta| > 0.119$, the solid state with constant orientation gradient ceases to exist, and the only possible solution is the liquid state. The undercooling is taken equal to 0.1 ($u = -0.1$). (b): curve $E = f(L)$ for $\Delta\theta = .1$ for the same parameters as in (a). Inset: blowup of the vicinity of the maximum.

fig. 1) by solving $V_{\text{eff}}(1) = V_{\text{eff}}(\phi_0)$. Then, the equilibrium solution (going from the middle of the grain boundary to the solid state on one side of the grain boundary) corresponds to the trajectory of a moving particle in V_{eff} that starts at the point B with zero velocity. Once $\phi(x)$ for the equilibrium solution has been computed, $\theta(x)$ is given by Eq. (11), and the total angle variation through the grain boundary can be obtained by simple integration. In order to compute the grain boundary solution for a given misorientation, the proper value of C has to be found, for instance by using a Newton-Raphson method.

In figure 3(a) we present a grain boundary solution for the same total angle variation $\Delta\theta = 0.6$ for $\alpha = 2$ and $\alpha = 3$ (in the calculations for $\alpha = 3$, we use the coupling function g of Eq. (9), changing just the exponent). As predicted, the angle variation is concentrated in the vicinity of the minimum of ϕ (the turning point B), and is very small outside the region where ϕ differs from 1. This indicates that this is indeed a localized grain boundary solution.

Using the computed solutions, the grain boundary energy is given by

$$E_{GB} = \int dx \left[\frac{1}{2}(\nabla\phi)^2 + V(\phi, T) + g(\phi)(\nabla\theta)^2 \right]. \quad (25)$$

(recall that we have chosen the homogeneous solid with-

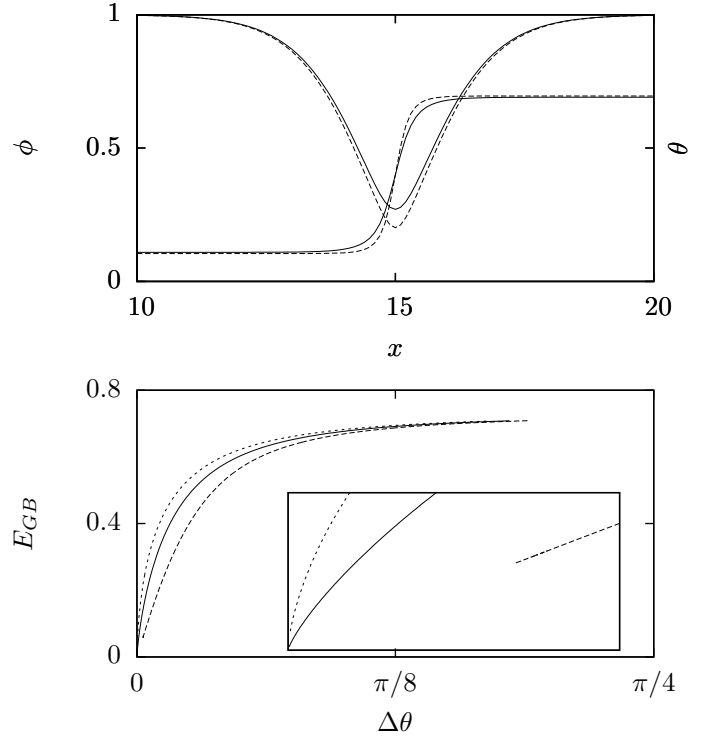


FIG. 3. (a): typical grain boundary profiles for the same misorientation ($\Delta\theta = 0.6$) and two values of α : $\alpha = 2$ (full lines) and $\alpha = 3$ (dashed lines). The dimensionless undercooling is 0.1. (b): Grain boundary energy as a function of the misorientation $\Delta\theta$ for different values of α ($\alpha = 2, 3$ and 4). The inset displays a zoom around the origin and shows the singular behavior for $\alpha = 3$ and 4 and the fact that for $\alpha = 2$ there is a small band of misorientations for which no grain boundary solution exists. (Here $\mu^2 = 10$)

out any angle variation as the zero of the free energy density). We display this energy as a function of the total angle variation $\Delta\theta$ in Fig. 3 (b). In the cases $\alpha = 3$ and 4, for small values of $\Delta\theta$, the energy has a power law behavior ($E_{GB} \sim (\Delta\theta)^\gamma$, with $\gamma = 0.8$ and 0.66, respectively). When $\Delta\theta$ increases toward infinity (this is not absurd since we have previously rescaled $\Delta\theta$ by μ), the grain boundary energy converges toward a constant value.

In the case $\alpha = 2$, the grain boundary energy also converges toward a constant value when $\Delta\theta$ becomes large. However, the behavior at small misorientations is very different: for small values of $\Delta\theta$, the grain boundary energy decreases linearly with the misorientation, but there exists a minimal value $\Delta\theta_m$ for which a grain boundary solution can exist (see inset). In fact, in the following we show that there is no grain boundary solution with angle variation smaller than this value in the case $\alpha = 2$.

As mentioned earlier, for $\alpha = 2$, $\phi = 1$ is not a maximum of the effective potential V_{eff} for all values of C . More precisely, V_{eff} can be formally written as

$$V_{\text{eff}}(\phi) = (1 - \phi)^2 [-p(\phi, T) + C^2/f(\phi)], \quad (26)$$

where $p(T, \phi)$ is a function such that $p(\phi, T)(1 - \phi)^2 = V(\phi, T)$. Using the notations of Eq. (22), V_{eff} writes in the vicinity of $\phi = 1$:

$$V_{\text{eff}}(\delta) = \delta^2 \left(-a - d\delta + \frac{C^2}{1 + b\delta + c\delta^2} \right) \quad (27)$$

with $\delta = 1 - \phi$. It can be seen that the curvature of V_{eff} changes sign in $\phi = 1$ when C^2 becomes bigger than a . This means that $\phi = 1$ is now a local minimum of V_{eff} . This change can happen in two ways: either the effective potential becomes greater than zero for all $\phi < 1$ (the turning point B in Fig. 1(a) moves to the right of the point A), or a new maximum develops between the points A and B (this happens in our case, as illustrated in Fig. 4), which means that a zero of V_{eff} must cross the point A from above. It is straightforward to show that the latter always happens if $ab + d > 0$. This explains the threshold value for $\Delta\theta$: grain boundary solutions with finite $\Delta\theta$ exist until the new maximum appears. Beyond this point, no grain boundary solution connecting to $\phi = 1$ is possible any more.

We have also verified that all the grain boundary solutions found up to now can be reached by simple integration of the equations of motion, Eqs. (5) and (6), at constant temperature (the field u is held constant), when the system is started from a homogeneous solid (with a value of the phase field slightly lower than unity) and a step function in the angle field. The resulting stationary solutions as well as their energies are independent of the system size (for sufficiently large systems) and of the discretization used (for grid spacings Δx smaller than about $0.5 W$). This shows that the model formulation is robust, and that the basin of attraction of the grain boundary solutions is large enough to make the model suitable for simulations of polycrystals.

D. Temperature dependence of the grain boundary solutions

In order to better characterize the model, we find it useful to explore the temperature dependence of the grain boundary solutions. We start out with the regime that should be of most practical interest, namely temperatures below the melting point ($T < T_m$, $u < 0$).

From the discussion of the preceding section, it is clear that the minimal grain boundary angle strongly depends on the behavior of $V(\phi)$ close to the solid state. Since we have chosen $V(\phi)$ such that the solid well is independent of temperature, the small-angle solutions should not be much affected by temperature changes. The same argument indicates that changes in undercooling (increasing undercooling) should only appreciably modify the high-angle grain boundaries and their energies. Simulation results show that this is indeed the case (see Fig. 5). As expected, for the double-well function of Eq. (10) that was designed to maintain the combination $ab - d$ constant (see appendix A), the minimal grain boundary

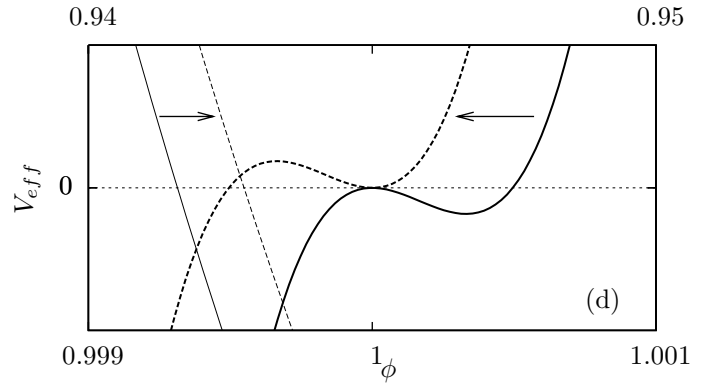


FIG. 4. Effective potential V_{eff} for $\alpha = 2$ and two values of C : $C = 1 \pm 5 \times 10^{-4}$ (dashed and solid lines, respectively). The thin lines correspond to the interval $0.94 < \phi < 0.95$ (upper axis) and display the turning point of the effective potential. The thick lines correspond to the interval $0.999 < \phi < 1.001$ (lower axis) and display the vicinity of the solid state. The arrows indicate the direction of change when C is lowered. It can clearly be seen that the turning point undergoes no qualitative change, whereas a new maximum appears close to $\phi = 1$ due to the fact that a zero of V_{eff} has crossed the point $\phi = 1$.

angle $\Delta\theta_m$ is found to be independent of undercooling. The grain boundary energy for small angles is also almost independent of temperature (see Fig. 5 (b)). For high-angle grain boundaries, the grain boundary energy depends roughly linearly on the undercooling, which is expected since for such boundaries the center of the grain boundary is almost in the liquid state ($\phi \approx 0$), and the free energy difference between solid and liquid is proportional to $T - T_m$.

We now turn to the case of negative undercooling (overheated solids). Whereas it is difficult if not impossible to overheat solids in experiments, due to the fundamental asymmetry between solidification and melting (for a review, see [24]), the existence of grain boundary solutions above the melting point has recently been actively discussed in the context of grain-boundary pre-melting, due to new results coming from molecular dynamics [25, 26] and phase-field crystal [27, 28] simulations. It has also been examined in orientation-field [15, 18] and multi-phase-field models [29–31]. It seems therefore useful to analyze our model in the light of this discussion.

A grain boundary can formally be described as two solid-liquid interfaces separated by a thin disordered (almost liquid) layer. The behaviour of a grain boundary when the melting point is approached then depends on whether the grain boundary energy is larger or smaller than the excess free energy of two solid-liquid interfaces. In the former case, the grain boundary is *repulsive*, since at the melting point, where the free energy density of both phases is equal, it is advantageous to separate the two solids by a macroscopic liquid layer. In the latter case, the grain boundary is *attractive*, since it is favor-

able for the two solids to stick together. More quantitatively, the total free energy excess of the grain boundary can be described as twice the solid-liquid surface free energy plus a so-called *disjoining potential*, which describes the interaction between the two interfaces as a function of their distance. In the classic theory of grain boundary premelting, this disjoining potential is assumed to be a simple exponential (see for example [29]), but it was shown that this simple form is not sufficient to describe low-angle grain boundaries in the phase-field crystal model [28]. Indeed, for these boundaries the interaction is attractive for large separations, but repulsive for short ones. As a consequence, equilibrium grain boundaries of finite width can exist at and above the melting point. It was later shown that such behavior (long-range attraction and short-range repulsion) is also generic for the standard multi-phase-field models (see [31] for a detailed discussion).

In our model, the structure of the solution space can be directly and simply deduced from the effective potential and the relation between the constant C and the total angle variation $\Delta\theta$. Let us start out by a brief discussion of the solutions that exist when the angle variation is zero. In this situation, $\partial_x\theta$ is zero everywhere, which implies $C = 0$, and the effective potential is just the negative of the double-well potential. For $T < T_m$, the solid has a lower free energy than the liquid, which implies that the solid maximum in the effective potential is higher than the liquid one. Therefore, no turning point exists, and no grain boundary solution of the type outlined above is possible. For $T > T_m$, the liquid maximum in V_{eff} is higher than the solid one, and therefore there always exists a turning point. The corresponding grain boundary solution is unstable. Indeed, it can be seen as a thin layer of liquid sandwiched between two solids, in a situation where the attraction between the two solid-liquid interfaces is exactly balanced by the free energy difference between solid and liquid. Hence, this solution corresponds to a saddle point of the free energy, which can be seen as a one-dimensional liquid nucleus. When the melting point is approached from above, the thickness of the liquid layer diverges, and the grain boundary energy approaches twice the solid-liquid surface tension.

Next, consider the situation when $T < T_m$. If the angle variation is finite, the constant C differs from zero, and the effective potential has two contributions. Since $g \rightarrow 0$ for $\phi \rightarrow 0$, the second term in Eq. (16) diverges in this limit. In addition, since g diverges for $\phi \rightarrow 1$, $1/g$ vanishes for $\phi \rightarrow 1$. Since C^2/g is positive, there is necessarily at least one solution for the equation $V_{\text{eff}}(\phi_0) = V_{\text{eff}}(1)$, which implies that there is a turning point for any value of C . It remains to link the values of C to the total angle variation. Whereas we did not find an analytical expression for this relationship, the main trends can be extracted from an analysis of the trajectory close to the turning point. When T tends to the melting temperature, the constant C necessarily becomes small since the liquid maximum in the returned double-

well potential lies closely below zero. This implies that the turning point is very close to the liquid state. As a consequence, g is also small, and the orientation gradient becomes large. Since g behaves like a power law with exponent larger than one close to the liquid state (see appendix A), the gradient at the center of the boundary becomes larger when C becomes smaller. Therefore, arbitrarily large total angle variations can be achieved for any temperature below T_m .

This situation changes when $T > T_m$: now, the liquid maximum in the returned double-well potential is higher than zero, which means that a turning point exists even for $C = 0$. When a non-zero value is chosen for C , this turning point moves further away from the liquid state. Therefore, the phase field remains finite in the center of the grain boundary, and the orientation gradient in the center of the grain boundary tends to zero when $C \rightarrow 0$. In this case, the curve of $\Delta\theta$ versus C is non-monotonous and presents a maximum. This implies that there is a maximum misorientation beyond which no grain boundary solutions exist. This maximum misorientation depends on the temperature and tends to infinity when $T \rightarrow T_m$. For misorientations smaller than this critical value, there are two distinct solutions. The solutions for C smaller than the maximum correspond to unstable liquid nuclei, whereas the solution branch for C larger than the maximum connects to the stable grain boundary solutions discussed previously. Solutions corresponding to a grain boundary and an unstable liquid nucleus are shown on Fig. 5 (d). While the angle profile is extremely similar in both cases, the liquid nucleus solution has a much smaller minimal ϕ . When the energies are plotted versus misorientation, the two branches meet at a cusp, as shown in Fig. 5 (b). At a fixed misorientation above the minimal value discussed previously $\Delta\theta_m$, there are thus stable grain boundary solutions for any $T < T_m$, and for a range of temperatures $T > T_m$ that depends on the misorientation. This overheated range tends to zero when the misorientation becomes large.

The stable grain boundary solutions all exhibit a deviation of the phase field from the solid state ($\phi = 1$), which can be interpreted as a thin layer of liquid by performing a Gibbs construction as in Ref. [28]. The existence of such a layer of finite thickness results from the interplay between two antagonistic effects, which can be understood through the interpretation of the grain boundary as two solid-liquid interfaces that come close together. On the one hand, the overlap of the two phase-field “tails” of the two interfaces creates an attractive force that would eliminate the liquid layer (as is happens in the case of zero misorientation). On the other hand, the finite total misorientation generates a restoring force that opposes this compression of the liquid layer: if the two interfaces get closer together, the orientation gradients have to increase. On the branch on solutions that is stable, this increase of the gradient leads to an increase of the free energy of the grain boundary solution, whereas the opposite is true on the unstable branch.

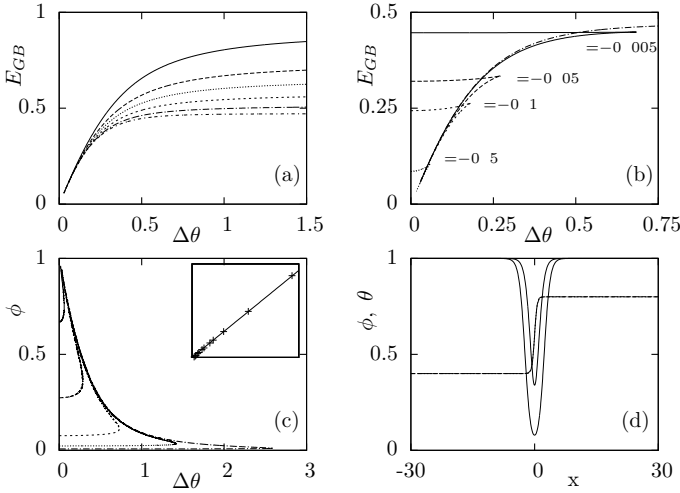


FIG. 5. **(a)** : Grain boundary energy as a function of $\Delta\theta$ for different values of the undercooling. The dash-dotted curve corresponds to $u = 0$. **(b)** : Grain boundary energy as a function of misorientation for overheated grain boundaries ($u > 0$, negative undercooling). Grain boundary solutions exist only for a finite range of misorientations. **(c)** : minimal value of ϕ in the grain boundary in the case of overheated grain boundaries, as a function of $\Delta\theta$, inset: value of the maximal angle variation through a stable grain boundary as a function of $u^{-1/4}$. **(d)** : ϕ (solid) and θ (dashed) as a function of x along both a grain boundary and a one-dimensional liquid nucleus for the same angle variation $\Delta\theta = 0.4$ and $u = 0.005$.

As a result, all the grain boundaries in our model are attractive. This finding coincides with the classic criterion. Indeed, the solid-liquid surface tension can be calculated analytically in our model and is equal to $\gamma_{sl} = \sqrt{2}/6$. The curve of E_{GB} versus $\Delta\theta$ at $u = 0$ ($T = T_m$), shown in Fig. 5, has an asymptote that tends exactly to $2\gamma_{sl} = \sqrt{2}/3 \approx 0.4714$ from below, which corresponds to two solid-liquid interfaces with a weak attractive interaction that is mediated by the exponential tails of the interfaces (see below). This behavior cannot easily be changed in our model. For example, the method used in Ref. [31] to make the interfaces repulsive is not applicable here because it requires a free energy density with minima in both field variables, which is not allowed if θ is to be interpreted as an orientation and rotational invariance is desired.

More complex behavior has been found in other orientation-field models [15, 18] by a suitable tuning of the various coupling functions. In particular, for certain temperature ranges the possibility of coexistence between two different grain boundary states was found. Similar behavior could probably be generated in our model if the double-well potential and the coupling function $g(\phi)$ are modified, but this issue is not pursued any further here.

To summarize, the model presented here with an appropriate choice of the coupling function and double-well potential has stable localized grain-boundary solutions

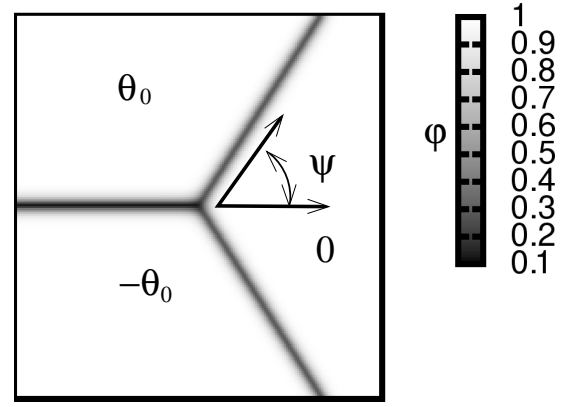


FIG. 6. Grey scale plot of ϕ for an equilibrium trijunction. The three grains with respective grain orientation θ_0 , $-\theta_0$ and 0 correspond to the white regions, and the grain boundaries correspond to the dark region. Here, $\theta_0 = 10^\circ$, the undercooling was 0.085, and $\mu^2 = 11.2$.

with an angle variation bigger than a threshold value (that can be made as small as desired by a proper choice of the quantity $ab + d$). It also has solutions that correspond to a homogeneous solid with constant gradient in crystal orientation as long as this gradient is smaller than a threshold value. For a given total angle variation, the free energy of the grain boundary is always smaller than the energy of the homogeneous solution (which may be metastable).

E. Trijunction points and Young's law

We have also checked explicitly that Young's law is satisfied at trijunction points. In order to obtain a static trijunction and to avoid curvature effects induced by simple Neumann boundary conditions, the simulation was performed as follows: first, we let three initially circular grains grow in a simulation box with Neumann boundary conditions. When the grains have impinged on the system boundaries, we use the value of the fields at the boundary at a certain time as Dirichlet boundary condition for the further evolution, which imposes that neither the phase field nor θ evolves any further at the boundary. This amounts to pinning the grain boundaries at fixed points of the system boundary. For initial orientations of the three grains given by θ_0 , 0, and $-\theta_0$ as displayed in Fig. 6, Young's law predicts

$$\psi = \arccos \left(\frac{E_{GB}(2\theta_0)}{2E_{GB}(\theta_0)} \right), \quad (28)$$

where ψ is the half of the dihedral angle, as sketched in Fig. 6; $E_{GB}(\theta_0)$ and $E_{GB}(2\theta_0)$ are the energies of grain boundaries with misorientations θ_0 and $2\theta_0$ that have been calculated in the previous subsection. For $\theta_0 = 4.2^\circ$ (resp. 10°), the angle ψ was 46° (resp. 55°), to be compared to 46° (resp. 52.4°) predicted from Young's

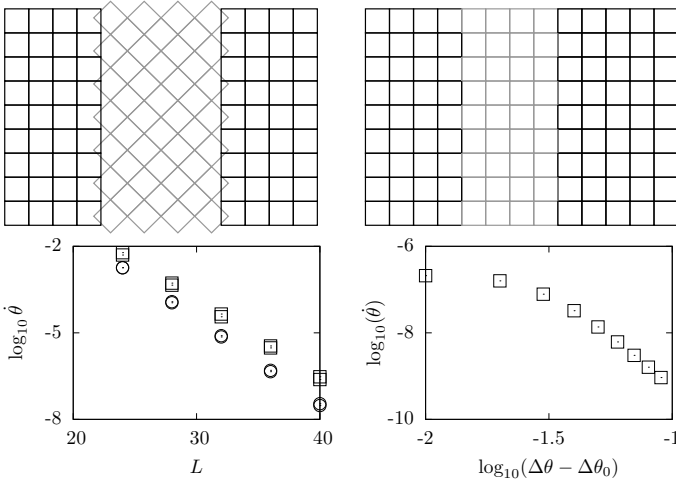


FIG. 7. **Top:** Sketch of the tricristal configuration, which can evolve towards a homogeneous system by the rotation of the central slab. **Bottom:** Rotation rate of the central slab as a function of distance between the boundaries for two different values of the angle difference through the grain boundary ($\Delta\theta$) (left) and as a function of misorientation ($\Delta\theta$) for a given value of the distance between the two grain boundaries (right). In these simulations, the orientation of the outer grains is kept constant.

law. The agreement is excellent, which is not surprising because Young’s law should generally be valid in phase-field models that derive from an energy minimization [32].

F. Grain boundary tails and the tricristal

Next, we briefly examine the interaction of two grain boundaries in the *tricristal* configuration sketched in Fig. 7: two grains of the same orientation sandwich a slab of material with a different orientation. The two grain boundaries obviously contribute a finite free energy. Since the evolution of the system is variational according to Eqs. (5) and (6) and nothing in the equations forbids the central crystal slab to rotate, the system tends to eliminate these defects: the orientation of the central slab slowly changes with time to approach the one of the outer grains, until the angle field finally becomes homogeneous. Obviously, for the sketched geometry this change cannot correspond to rigid body rotation. The evolution equation for the orientation actually describes the *local* rotation of disconnected objects, such as the molecules of a liquid crystal. For a continuously connected rigid solid, such a rotation could only be accomplished by a change in local connectivity, obtained for example by the migration of dislocations from one grain boundary to the other (see [33] for a more detailed discussion). However, since this process (if it takes place at all) would be extremely slow, the rotation of the central slab should be suppressed. In the previous orientation-field models that contain a mod-

ulus of the gradient in the free energy functional, this is problematic since the functional derivative has a singularity at the points with vanishing orientation gradients – that is, inside the grains. The singular diffusion equation that results from the functional derivative leads to a non-local coupling of the grain boundaries [22]. As a consequence, the rate of rotation of the central crystal slab does not depend on the distance between the grain boundaries. Therefore, the only solution to suppress the unwanted rotation is to choose a mobility function which vanishes inside the crystal grains [16].

In our model, the interaction between the grain boundaries is local. This can be easily demonstrated by an analysis of the “tails” of the boundary, that is, the approach of the phase and orientation fields to their bulk values. This is again straightforward by using the mechanical analog. Indeed, a linearization of Eq. (15) in the vicinity of the solid state yields

$$\phi_{xx} = - \left. \frac{\partial^2 V_{\text{eff}}}{\partial \phi^2} \right|_{\phi=1} (\phi - 1), \quad (29)$$

the solution of which is

$$\phi(x) = 1 - A \exp[\pm \xi(x - x_0)] \quad (30)$$

with $\xi = \sqrt{(\partial^2 V_{\text{eff}})/(\partial \phi^2)|_{\phi=1}}$, and the values of the integration constants A and x_0 as well as the sign inside the exponential are fixed by the boundary conditions (which depend on the position of the grain boundary). The gradient in orientation is then obtained from Eq. (13) and tends to zero in the grains since $g(\phi)$ diverges as $\phi \rightarrow 1$.

Several conclusions can be drawn from this result. First, the grain boundaries in our model are truly localized, in the sense that in a heterogeneous system only an exponentially small part of the orientation variation takes place outside the grain boundaries. Second, the interaction between two grain boundaries decays exponentially with their distance for well-separated grain boundaries, since for large separation the interaction is mediated by the overlap of the exponential tails (see [31] for a more detailed discussion). As a consequence, even for a constant mobility in the orientation evolution equation ($Q(\phi, \nabla\theta) = 1$), the rotation rate of the central slab in the tricristal configuration should rapidly drop with the size of the slab. Finally, the characteristic length of decay for the exponential tails $1/\xi$ is the inverse of the second derivative of the effective potential, taken in the solid state. As discussed above, the second derivative depends of the value of the constant C and vanishes at a critical value of C that corresponds to the minimal misorientation $\Delta\theta_m$. Therefore, grain boundaries with smaller misorientations interact more strongly.

These predictions are borne out by simulations on the tricristal configuration, as shown in Fig. 7. For grain boundaries of a fixed misorientation, the rotation rate of the central slab decays exponentially with systems size (and thus, separation of the grain boundaries), and the

rotation rate is larger for smaller misorientations at a fixed separation. Therefore, while our model does permit grain rotation, qualitatively by the same mechanism than in previous orientation-field models, the artefacts introduced by this design are small even for a constant mobility function, and it can be hoped that they will not drastically affect the results of large-scale simulations.

III. ANISOTROPIC INTERFACES

Our model can describe two different types of boundaries: solid-liquid interfaces and grain boundaries, both of which are in general anisotropic. For solid-liquid interfaces, the surface tension and interface mobility depend on the orientation of the interface with respect to the crystal axes of the solid. For grain boundaries, the energy and mobility depend on the orientation of *both* crystals that meet at the boundary. This yields two independent parameters in two dimensions, and five independent parameters in three dimensions. Grain boundary energies and mobilities are conventionally given as functions of the *misorientation* between the two crystals and the *inclination* of the grain boundaries.

The standard way of including the anisotropy of the solid-liquid interfaces in phase-field models is to make the coefficient of the phase-field gradient term dependent on the interface orientation (see for example [34]). We will now explore the effects of introducing this type of anisotropy in our model. As we will see below, the modification of the phase-field gradient term also makes grain boundaries anisotropic. Since the anisotropies in both types of boundaries are created by one single term in the free energy functional, they are obviously not independent. A possible way to choose both anisotropies independently would be to introduce a suitable dependence on orientation in the coefficient of the orientation-field gradient term. However, this possibility will not be explored further here.

For a crystal of a cubic material in two dimensions with its crystallographic axes aligned with the coordinate system, the orientation-dependent surface tension is usually written as

$$\gamma(\varphi) = \gamma_0 [1 + \epsilon_4 \cos(4\varphi)], \quad (31)$$

where φ is the angle between the interface normal (pointing into the liquid) and the x axis. If the crystal is rotated by an angle θ , this expression becomes

$$\gamma(\varphi, \theta) = \gamma_0 [1 + \epsilon_4 \cos[4(\varphi - \theta)]] . \quad (32)$$

To implement this anisotropy in the phase-field model, we define the unit normal vector by $\mathbf{n} = -\nabla\phi/|\nabla\phi|$ and choose the gradient coefficient to be

$$W_\phi(\mathbf{n}, \theta) = W_0 a(\mathbf{n}, \theta) \quad (33)$$

with the anisotropy function

$$a(\mathbf{n}, \theta) = 1 + \epsilon_4 [\cos(4\theta) (4n_x^4 + n_y^4) - 3] + \sin(4\theta) (4n_x n_y^3 - 4n_y n_x^3), \quad (34)$$

where we have repeatedly used the addition theorems for the trigonometric functions. Lengths are now scaled by the average interface thickness W_0 .

A few consequences of the fourfold symmetry should be mentioned here. The fundamental issue is that for a cubic material all orientations that differ by integer multiples of $\pi/2$ are equivalent. Indeed, a crystal unit cell can be locally rotated by a multiple of $\pi/2$ without changing the state of the crystal. Therefore, θ is actually defined modulo $\pi/2$, which means that the values of θ can be restricted to the interval $[0, \pi/2[$. This means that, contrary to what we did in the previous section, we cannot rescale θ to make $\mu = 1$. Nevertheless, we will consider in the following the case $\mu = 1$ for simplicity. Furthermore, care has to be taken in the calculation of differential operators. For instance, in the evaluation of the gradient energy and in the Laplace operator, differences between the values of θ at neighboring grid points need to be computed. We follow the method proposed in Ref. [20]: in the evaluation of such operators for a given grid point i , we check for each neighboring point which of all the equivalent values of θ gives the lowest value of the gradient energy, and calculate the evolution of point i using this value. This procedure ensures that local “jumps” of the angle field with amplitude $\pi/2$ (or multiples of it) do not introduce any energy cost. Thus, all the crystal symmetries are correctly implemented. Nevertheless, for simplicity of exposition, we will use the standard notation for differential operators in the remainder of the paper.

The evaluation of the variational derivatives in Eqs. (5) and (6) yields

$$\begin{aligned} P(\phi, \nabla\theta) \partial_t \phi &= \nabla \cdot [a(\mathbf{n}, \theta)^2 \nabla \phi] \\ &+ \partial_x \left(|\nabla\phi|^2 a(\mathbf{n}, \theta) \frac{\partial a(\mathbf{n}, \theta)}{\partial(\partial_x \phi)} \right) \\ &+ \partial_y \left(|\nabla\phi|^2 a(\mathbf{n}, \theta) \frac{\partial a(\mathbf{n}, \theta)}{\partial(\partial_y \phi)} \right) \\ &- V'(\phi, T) - \mu^2 (\nabla\theta)^2 g'(\phi) \end{aligned} \quad (35)$$

and

$$Q(\phi, \nabla\theta) \partial_t \theta = \mu^2 \nabla \cdot (g(\phi) \nabla \theta) - a(\mathbf{n}, \theta) \frac{\partial a(\mathbf{n}, \theta)}{\partial \theta} (\nabla\phi)^2. \quad (36)$$

For a uniform (constant) orientation field, the first of these equations is identical to the standard anisotropic phase-field equation of Ref. [34], with the crystalline axes rotated by the angle θ away from the x axis. The equation for the orientation field contains the derivative with respect to the angle of the phase-field gradient coefficient. Physically, this term represents a “torque” exerted on the orientation field at the surface. Indeed, if the solid-liquid interface is anisotropic, this term drives the angle field towards an orientation which corresponds to a minimum of the surface free energy.

In the following, we will examine in more detail the influence of the new terms on grain boundaries, solid-liquid interfaces, isolated monocrystals and polycrystals.

A. Grain boundaries

We have systematically calculated stationary one-dimensional grain boundary solutions of the anisotropic equations (35) and (36), and determined the grain boundary energy. The results are presented in Fig. 8. As stated above, in two dimensions, there are two independent parameters. For two grains of respective orientations θ_1 and θ_2 , we define the misorientation, as before, as $\Delta\theta = \theta_2 - \theta_1$, and the median angle as $\theta_{\text{mid}} = (\theta_1 + \theta_2)/2$.

The curve of the grain boundary energy versus the median orientation for a fixed misorientation exhibits the expected behaviour, that is, a 4θ dependence shown by the $\pi/2$ periodicity of the grain boundary energy as a function of θ_{mid} . We limit ourselves to inclinations that are smaller than $\pi/2$ since other values can be reached by symmetry. It is also interesting to note that higher misorientations can have a lower grain boundary energy for certain inclinations. This is due to the fact that a grain boundary consists, roughly speaking, of two solid/liquid interfaces and that changing the inclination rotates both of these interfaces with respect to the orientation of the crystalline axes. This can lead to decrease of the energetic cost that can be higher than the increase due to an increase of the misorientation.

It should be mentioned that in our first implementation of the model, we noticed a very slow motion of one-dimensional anisotropic grain boundaries [35]. This is clearly unphysical since the free energy density in the grains on both sides is identical, which precludes a persistent motion to one side. We found that this effect was due to the discretization. Indeed, the anisotropic terms lead to assymetric ϕ profiles at the grain boundary since the grain orientation relative to the grain boundary normal is, in general, not the same on both sides of the interface. Therefore, the unavoidable discretization errors present on both sides of the boundary do in general not exactly compensate each other, which then leads to an unwanted movement of the interface. We eliminated this problem by changing the discretization scheme: instead of discretizing the equations of motion (35) and (36), we discretized the free energy functional and replaced the functional derivatives by ordinary derivatives. As a result, we obtain discrete equations that derive from a discrete energy function. It can easily be shown (see appendix B) that with this scheme the energy function is strictly decreasing with time; indeed, no spurious motion of the grain boundaries took place with this modified scheme.

B. Solid-liquid interfaces and equilibrium crystal shapes

Next, we turn to the study of solid-liquid interfaces. Bulk liquid and solid coexist at the melting point ($T = T_m$, $u = 0$), which implies that there must exist an equilibrium solution for a planar interface. For a constant

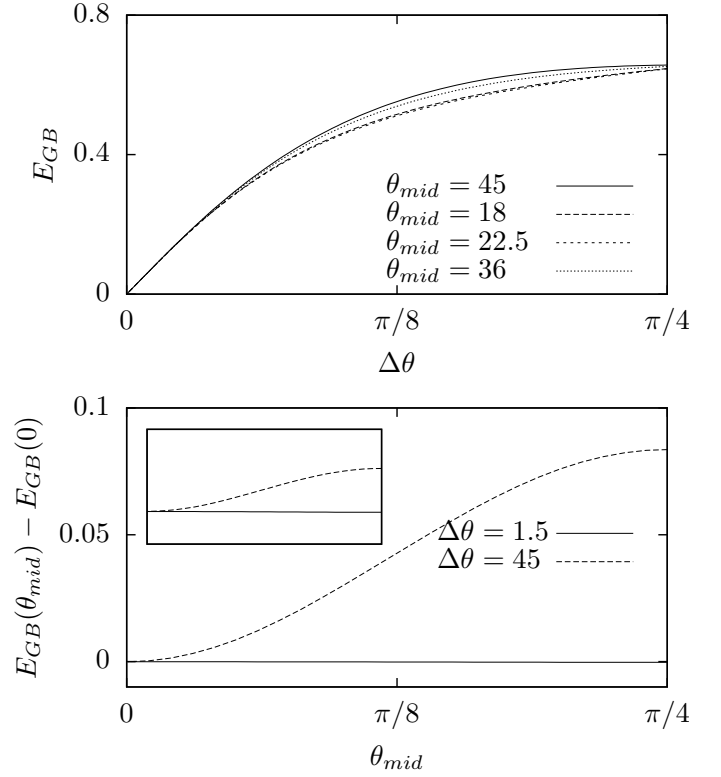


FIG. 8. **Top:** Grain boundary energy as a function of the misorientation for different values of the median angle ($\epsilon = 0.05$, $u = -0.1$). **Bottom:** grain boundary energy as a function of the median angle for two different values of the misorientation. Inset: same curves, normalized by the minimal energy of such a GB (≈ 0.5 for the case where the misorientation is 1.5° and ≈ 3.2 for a 45° misorientation). Clearly, for small values of the misorientation, the grain boundary energy is less sensitive to anisotropy than for high values.

orientation field ($\theta(\mathbf{x}) = \theta_0$), this solution (for an interface normal to the x direction and centered at position x_0 , with the solid located in the domain $x < x_0$) can be obtained analytically and reads

$$\phi(x) = \frac{1}{2} \left[1 - \tanh \left(\frac{x - x_0}{\sqrt{2}W_\phi(\theta_0)} \right) \right]. \quad (37)$$

This interface has a surface free energy of $\gamma = \gamma_0 W_\phi(\theta_0)/W_0$, which has already been used to choose W_ϕ in Eq. (33).

However, a constant orientation field is a stationary solution of the anisotropic orientation equation (36) only if the angle θ_0 corresponds to symmetry direction of the crystal (a minimum or maximum of the anisotropy function). In all other cases, the “torque” term is non-zero inside the interface, which generates an evolution of the orientation if the system is started from a constant orientation field.

This effect is actually not physical for a crystalline material. It is completely analogous to the *anchoring* effect known for liquid crystals. Indeed, in such materials,

the constituent molecules are anisotropic and exhibit an orientational order, but are free to rotate individually. Therefore, if the surface energy depends on the orientation of the molecules with respect to the surface normal, a competition between bulk and surface effect takes place. Any variation of the orientation in the bulk is energetically penalized, but the energy gain due to the surface terms can offset this penalty for molecules close to the surface, such that the orientation tends to an energetically favorable direction close to the surface. In contrast, in a crystalline material, the structure cannot change by rotation of the individual crystalline unit cells. The interface orientation can change only by attachment and detachment of atoms.

To eliminate this effect, existing orientation-field models adopt a radical strategy [17]: they just set the “torque” term to zero and use Eq. (36) with only its first term on the right hand side. Whereas this procedure can be justified by the arguments given above, it breaks the variational structure of the model, which means that several desirable mathematical properties are lost (in particular, the free energy is not guaranteed to decrease with time any more). Instead of adopting the same strategy in our model, we will proceed by showing that the effects induced by this surface term are actually small. Once again, the facts that the diffusion part of the orientation equation is *regular* and that the orientation variation is localized in the vicinity of the interfaces are crucial for this property of the model.

When we start the two coupled equations (35) and (36) from the solution given by Eq. (37) at a fixed temperature $u = 0$, we observe that the solid grows very slowly at the expense of the liquid. This can be qualitatively understood by the following reasoning. As mentioned above, the torque term induces an evolution of the orientation field towards a more favorable direction. If the solid could “turn” by changing its orientation, the system would be able to reach its global energy minimum (the orientation field aligned with a direction of minimal surface tension). However, since the gradient of orientation tends exponentially to zero away from the interfaces, there is actually no term in the orientation equation which could induce such a rotation. However, the system can lower its energy by moving the interface and simultaneously changing the orientation field inside the interface. In this way, a homogeneous liquid is successively replaced by a solid with a very small “frozen in” orientation gradient that results from the time evolution of the surface orientation. This “strained” solid has a higher free energy density than the liquid, but this can be offset by the lowering of the surface free energy, such that the total energy of the system still decreases.

In summary, the anisotropy of the solid-liquid interface induces an unphysical growth of the solid at the melting temperature. In other words, the presence of the additional degree of freedom (change in orientation) leads to a shift of the melting point for anisotropic interfaces. To quantify the importance of this effect, we have deter-

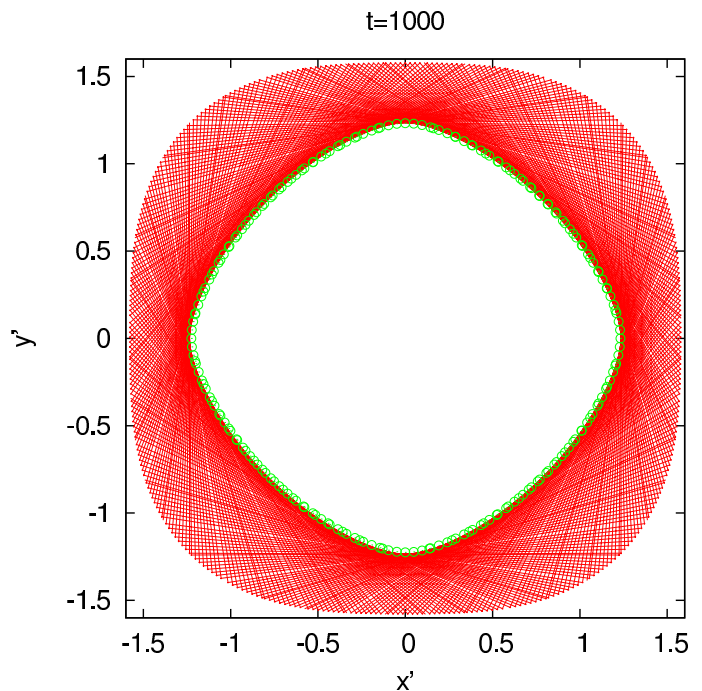


FIG. 9. (Color online) The equilibrium shape of an anisotropic crystal (green circles) agrees well with the Wulff shape (inner envelope of the red lines). The anisotropy is $\epsilon_4 = 0.05$.

mined the modified melting temperature by performing simulations at constant volume of solid, as described in appendix C. The shift is actually very small, of the order of $u \sim 10^{-4}$. Moreover, since the profile of phase field and orientation across the interface are not exactly given by Eq. (37), the actual surface tension slightly differs from the intended value. To test the magnitude of this effect, we have determined the equilibrium shape of a two-dimensional anisotropic crystal, again by performing simulations at constant volume of solid. In Fig. 9, we show the resulting equilibrium shape and the comparison to the Wulff construction, which is very satisfactory. Indeed, for typical undercoolings that can be reached in simulations ($u \sim 0.1$), the shift of the equilibrium point is negligibly small, and therefore it is not surprising that the model is capable of producing an excellent approximation to the equilibrium crystal shape.

We have not explicitly checked Young’s law at trijunction points for the anisotropic version of our model. However, it is shown in Ref. [32] that Young’s law is generally valid for phase-field models that are variational, since equilibrium states result from an energy minimization. Since this is the case for our model, and the equilibrium crystal shape is well reproduced, we are fairly confident that our model also correctly implements the balance of Herring torque terms at trijunction points.

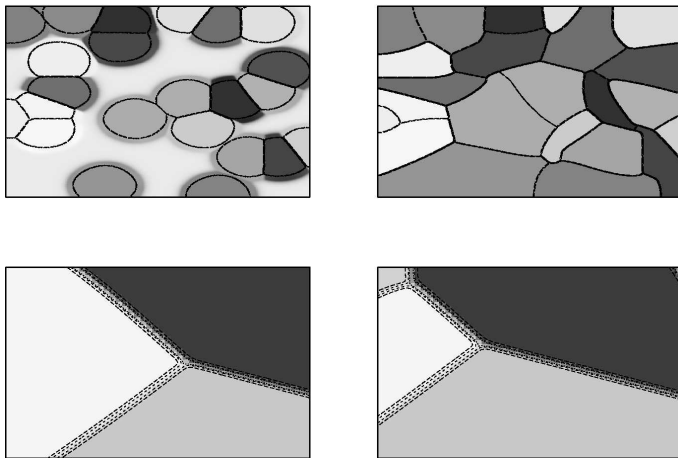


FIG. 10. Snapshots of the numerical simulation of the isothermal growth of multiple grains. The grey scale indicates the orientation of grains. The undercooling is kept homogeneous and constant and the initial grains (top left) grow until they begin to interact with each other (top right). Once all the liquid is transformed, the further evolution is only driven by differences in grain boundary energies and becomes much slower. As one can see, most grain boundaries are already straight (especially high angle grain boundaries between dark and light regions). A typical change in structure is shown in the two plots at the bottom: snapshots at two successive times of the same region (only a small part of the system is shown) are displayed. Between the two snapshots, the length of the high angle grain boundary (between the dark and light region) has significantly decreased, which has led to a motion from right to left of the triple junction.

C. Polycrystals

We now turn to a more illustrative part, where we show results of numerical simulations for the case of isothermal solidification (that is, we set u to a constant that does not evolve with time). The aim is to show that our model is capable of reproducing the evolution of polycrystals, at least qualitatively. Hence, we have simulated the solidification of an undercooled melt with a few seeds of different crystalline orientations. The result is shown in Fig. 10. First, the individual grains grow. Since we do not solve the heat equation (8), no diffusive instability can appear and create dendrites, and the shape of the grains remains convex. Once the grains impinge, grain boundaries appear. They evolve toward straight segments, the lengths of which change through the motion of triple junctions while the orientation in each grain remains unchanged. Other situations such as directional solidification in a fixed temperature gradient were also simulated, and also led to qualitatively correct behaviour of the model.

IV. CONCLUSION

We have presented a phase-field model for the solidification and coarsening of polycrystals that is formulated in terms of two continuous fields, a phase field that indicates the local state of matter and an orientation field that gives the local direction of the crystallographic axes. Contrary to previous orientation-field models found in the literature, the free-energy functional of our model does not contain a term proportional to the modulus of the orientation gradient, but only a standard square gradient term. Stable localized grain boundary solutions are instead generated by a singular coupling function between the orientation and the phase field.

As a result, the mathematical structure of the model and the evolution equations are closer to the standard phase-field models for solidification, in that the evolution equation for the phase field is a regular reaction-diffusion equation instead of a singular diffusion equation that has to be regularized in a suitable way. The properties of the grain boundary solutions can be investigated by standard mathematical methods, in particular by the use of the well-known mechanical analog that exploits the relation between interface solutions and the motion of a particle in a potential landscape. This method has allowed us to perform a thorough analysis of the grain boundary properties, and to choose a suitable mathematical form of the singular coupling function.

One important result of this analysis is that the grain boundary solutions of our model have a similar structure as the solid-liquid interfaces in standard phase-field models: a central region with strong gradients of both fields is surrounded by exponential tails, and the interaction between two grain boundaries becomes exponentially small with their distance. Two important differences with previous orientation-field models are a consequence of these facts. First, the artificial grain rotation that is mediated by long-range interactions between grain boundaries is not present in our model. Second, it is possible to incorporate interfacial anisotropy in our model without breaking the variational structure of the model. The anisotropy generates unphysical “torque” terms that drives the orientation fields towards the minima of the surface free energy, but these effects are negligibly small for typical simulation parameters that can be achieved in practice.

We have presented some preliminary simulations performed in two dimensions, which show that a qualitative description of multi-grain growth and of the evolution of polycrystalline solids can be obtained using this model. It should be stressed that the evolution equation for the orientation obtained from the variational formalism, Eq. (6), is likely to be incorrect, as discussed in more detail in Ref. [33]. Therefore, it is unlikely that this model can be used for quantitative simulations of grain growth. Nevertheless, in our opinion this model is interesting because of its intrinsic mathematical structure and because of its ability to reproduce a host of complex pattern-formation

phenomena with the help of a simple set of equations.

We have concentrated here on the discussion of the mathematical structure of the model, but we have neither tested its efficiency nor its quantitative accuracy in the case of known model problems, such as the growth of an isolated dendrite [34]. These are promising subjects for further studies.

Appendix A: Choice of model parameters: further details

The choice of the coupling function for values of the phase field close to one (the solid) has already been discussed in the main text. Here, we briefly discuss the form of the coupling function g close to zero and the double-well potential used in our simulations. First, g must be equal to zero in the liquid (there should be no energy penalty associated with orientation changes in the liquid phase). Furthermore, we must have $g'(0) = 0$ in order to keep a minimum of the free energy at the liquid state, irrespective of the configuration of the orientation field, which has no meaning inside the liquid. Finally, we also require that the variation of the orientation should remain confined in the grain boundary. A similar problem was solved in a phase-field model of fracture, where the strain must be localized inside the crack for a broken elastic material. According to the results of Ref. [36], this imposes that g should behave as ϕ^β for $\phi \rightarrow 0$, with $\beta > 2$. Choosing $\beta = 2$ would lead to a singular behaviour of θ in the middle of the grain boundary (and to strong pinning of the grain boundary on the grid points). Therefore, we choose $\beta = 3$.

The conditions on the double-well potential are the following: it should have two minima at $\phi = 0$ and $\phi = 1$ for all temperatures, with a free energy difference proportional to u between the two wells. Furthermore, its second and third derivatives in the solid should be con-

stant; this is guaranteed if its leading order expansion in $\phi = 1$ is of the form $(1 - \phi)^2 - 2(1 - \phi)^3$; with this choice, Eq. 23 is satisfied. In addition, we want to prescribe both the second derivative of the potential C_{liq} and its value V_0 in $\phi = 0$. The first is set to the same value as the second derivative in the solid well, in order to guarantee a symmetric interface profile of the phase field, and the second is a function of temperature, whereas the depth of the solid well is independent of temperature. Assuming that V has a polynomial form, the number of equation it has to satisfy is 7:

1. The free energy of the liquid phase is V_0 : $V(0, T) = V_0(T)$
2. The liquid phase is a minimum : $V'(0) = 0$
3. The curvature of the potential at $\phi = 0$ is fixed : $V''(0) = 2C_{\text{liq}}$
4. The free energy of the solid state is 0: $V(1) = 0$
5. $\phi = 1$ is a minimum : $V'(1) = 0$
6. The expansion of V in $\phi = 1$ has to be $(1 - \phi)^2 - 2(1 - \phi)^3$: $V''(1) = 2$ and $V^{(3)}(1) = 12$

The first 3 equations impose the value of the constant and of the coefficients ϕ and ϕ^2 in the polynomial expansion of $V(\phi)$, while the last four equations (the last three points of the above enumeration) can be easily translated into a set of four independent linear equations on the coefficient of V . An evident solution is then to consider that V is a 6th order polynomial and to solve the linear system imposed by the last four equations in order to compute the remaining coefficients of V . This approach leads to the following expression of V :

$$V(x) = V_0 + C_{\text{liq}}x^2 + cx^3 + dx^4 + ex^5 + fx^6. \quad (\text{A1})$$

The remaining 4 coefficients have then to satisfy a set of 4 independent linear equations that can be inverted giving the following polynomial form for V :

$$V(x) = U_{\text{liq}} + C_{\text{liq}}x^2 + cx^3 + dx^4 + ex^5 + fx^6. \\ \begin{pmatrix} c \\ d \\ e \\ f \end{pmatrix} = \frac{1}{6} \begin{pmatrix} 120 & -60 & 12 & -1 \\ -270 & 150 & -33 & 3 \\ 216 & -126 & 30 & -3 \\ -60 & 36 & -9 & 2/3 \end{pmatrix} \begin{pmatrix} -V_0 - C_{\text{liq}} \\ -2C_{\text{liq}} \\ 2 - 2C_{\text{liq}} \\ 12 \end{pmatrix} \begin{pmatrix} (V(1) = 0) \\ (V'(1) = 0) \\ (V''(1) = 2) \\ (V^{(3)}(1) = 12) \end{pmatrix} \quad (\text{A2})$$

Choosing to have $C_{\text{liq}} = 1$, we have:

$$V(\phi) = V_0 + \phi^2 - (2 + 20V_0)\phi^3 + (1 + 45V_0)\phi^4 - 36V_0\phi^5 + 10V_0\phi^6 \quad (\text{A3})$$

The choice of $V_0 = -\lambda u$ (which yields the correct free energy difference between the two bulk phases) gives Eq. (10). With this choice of V , a reasonable choice for g is

finally:

$$g = \frac{7\phi^3 - 6\phi^4}{(1 - \phi)^2} \quad (\text{A4})$$

Appendix B: Discretization issues

Here, we illustrate briefly how a discretization scheme that does not derive from an energy can lead to spurious motion of the interface while a discretization scheme that derives from a free energy cannot lead to any such effect. The free energy we consider (for simplicity, in one dimension) writes

$$\mathcal{F} = \int dx \varepsilon(\theta) \frac{(\nabla \phi)^2}{2} + V(\phi) + g(\phi)(\nabla \theta)^2 \quad (\text{B1})$$

When simulating the behaviour of a partial differential equation (PDE) that derives from this free energy, one can either first derive the PDE and then discretize it or first discretize the free energy and then derive the evolution equation for the discretized field. In the following, we consider both options and show how they differ in the case of the first term in the above functional. The evolution equation that derives from this term for the phase field ϕ is

$$\partial_t \phi = \partial_x (\varepsilon(\theta) \partial_x \phi) \quad (\text{B2})$$

$$= \varepsilon'(\theta) \partial_x \theta \partial_x \phi + \varepsilon(\theta) \partial_x^2 \phi, \quad (\text{B3})$$

where we have used the chain rule to obtain the second expression. The latter equation is simply discretized as follows:

$$\begin{aligned} \partial_t \phi_n &= \varepsilon'(\theta_n) \frac{(\theta_{n+1} - \theta_{n-1})(\phi_{n+1} - \phi_{n-1})}{4(\Delta x)^2} \\ &+ \varepsilon(\theta_n) \frac{\phi_{n+1} - 2\phi_n + \phi_{n-1}}{(\Delta x)^2} \end{aligned} \quad (\text{B4})$$

The other approach is to first discretize the free energy:

$$\mathcal{F}_d = \sum_n \frac{\varepsilon(\theta_{n+1/2})}{2} \left(\frac{\phi_{n+1} - \phi_n}{\Delta x} \right)^2, \quad (\text{B5})$$

where $\theta_{n+1/2}$ is either the value of θ on a staggered grid or the mean value of θ between the grid points. This, using the relaxation law $d\phi_n/dt = -\partial \mathcal{F}_d / \partial \phi_n$, leads to an evolution equation for ϕ_n that writes (taking into account all the terms of the sum):

$$\frac{d\phi_n}{dt} = \varepsilon(\theta_{n+1/2}) \frac{\phi_{n+1} - \phi_n}{(\Delta x)^2} + \varepsilon(\theta_{n-1/2}) \frac{\phi_{n-1} - \phi_n}{(\Delta x)^2} \quad (\text{B6})$$

This equation differs from Eq. (B4) by little. Indeed, it is easy to see that it corresponds to the discretization of Eq. (B2) instead of Eq. (B4). Using a Taylor expansion centered at the grid point n one can show that both discretization schemes are equivalent up to the second order, but differ by terms of higher order. This just reflects the

fact that the chain rule is valid for continuous fields, but not for discrete fields.

These seemingly small differences have important consequences. Due to its construction, Eq. (B6) implies that \mathcal{F}_d is decreasing with time:

$$\frac{d\mathcal{F}_d}{dt} = \sum_n \frac{d\phi_n}{dt} \times \frac{\partial \mathcal{F}_d}{\partial \phi_n} \quad (\text{B7})$$

$$= - \sum_n \left(\frac{d\phi_n}{dt} \right)^2 \leq 0. \quad (\text{B8})$$

Therefore, the free energy is guaranteed to decrease toward a minimum. Furthermore, the \mathcal{L}^2 -norm of the rate of change of ϕ is proportional to the rate of change of the discretized energy. This means that if the interface is moving, then its squared velocity is proportional to the rate of change of the free energy. In other words, any motion of the interface (whatever are the discretization errors) comes with a decrease in the free energy. This differs qualitatively from the expression of Eq. (B4) which *a priori* has no reason to derive exactly from any energy and where the interface can have a motion proportional to discretization errors, as was indeed found in our early investigations of this model [35].

Appendix C: Simulations at constant volume of solid

The discretized equation of motion for the phase field has the structure

$$\frac{d\phi_n}{dt} = A_n + B_n u_n, \quad (\text{C1})$$

where a one-dimensional example is considered for simplicity, A_n and B_n are coefficients that depend on the local configuration of phase and orientation fields, and u_n is the discretized temperature field. For a constant but time-dependent temperature, $u_n \equiv u(t)$, we have

$$\frac{d}{dt} \sum_n \phi_n = \sum_n A_n + u(t) \sum_n B_n. \quad (\text{C2})$$

The left hand side can be interpreted as the change in the total volume of solid. Clearly, $\sum_n \phi_n$ can be kept constant by the following procedure: (i) evaluate the coefficients A_n and B_n , (ii) calculate the temperature $u = -\sum_n A_n / (\sum_n B_n)$ which makes the left hand side vanish, and (iii) timestep the equations with this value of the temperature. After a short time, the temperature converges to a constant value, which corresponds to the equilibrium temperature for the chosen total volume of solid.

- [2] H. V. Atkinson. Theories of normal grain-growth in pure single-phase systems. *Acta Metall.*, 36:469–491, 1988.
- [3] C. V. Thompson. Structure evolution during processing of polycrystalline films. *Annu. Rev. Mat. Sci.*, 30:159–190, 2000.
- [4] W. J. Boettinger, J. A. Warren, C. Beckermann, and A. Karma. Phase-field simulation of solidification. *Annu. Rev. Mater. Res.*, 32:163–194, 2002.
- [5] Long-Qing Chen. PHASE-FIELD MODELS FOR MICROSTRUCTURE EVOLUTION. *Annual Review of Materials Research*, 32(1):113–140, August 2002.
- [6] I. Steinbach. Phase-field models in materials science. *Model. Simul. Mater. Sci. Eng.*, 17(7):073001, 2009.
- [7] I. Steinbach, F. Pezolla, B. Nestler, M. Seesselberg, R. Prieler, G.J. Schmitz, and J.L.L. Rezende. A phase field concept for multiphase systems. *Physica D*, 94:135–147, 1996.
- [8] D. Fan and L.-Q. Chen. Computer simulation of grain growth using a continuum field model. *Acta Mater.*, 45(2):611–622, 1997.
- [9] Britta Nestler, Harald Garcke, and Björn Stinner. Multi-component alloy solidification: Phase-field modeling and simulations. *Physical Review E (Statistical, Nonlinear, and Soft Matter Physics)*, 71(4):041609, 2005.
- [10] Seong Gyoon Kim, Dong Ik Kim, Won Tae Kim, and Yong Bum Park. Computer simulations of two-dimensional and three-dimensional ideal grain growth. *Phys. Rev. E*, 74:061605, 2006.
- [11] N. Moelans, B. Blanpain, and P. Wollants. Quantitative analysis of grain boundary properties in a generalized phase field model for grain growth in anisotropic systems. *Phys. Rev. B*, 78(2):024113, 2008.
- [12] L. Vanherpe, N. Moelans, B. Blanpain, and S. Vande-walle. Bounding box algorithm for three-dimensional phase-field simulations of microstructural evolution in polycrystalline materials. *Phys. Rev. E*, 76(5):056702, 2007.
- [13] R. Kobayashi, J.A. Warren, and W.C. Carter. Vector valued phase field model for crystallization and grain boundary formation. *PHYSICA D*, 119:415–423, 1998.
- [14] R. Kobayashi, J. A. Warren, and W. C. Carter. A continuum model of grain boundaries. *Physica D*, 140(1-2):141–150, 2000.
- [15] AE Lobkovsky and JA Warren. Phase field model of premelting of grain boundaries. *Physica D*, 164:202–212, 2002.
- [16] J. A. Warren, R. Kobayashi, A. E. Lobovsky, and W. C. Carter. Extending phase field models of solidification to polycrystalline materials. *Acta Mater.*, 51(20):6035–6058, 2003.
- [17] L. Gránásy, T. Pusztai, and J. A. Warren. Modelling polycrystalline solidification using phase field theory. *J. Phys. – Cond. Mat.*, 16(41):R1205, 2004.
- [18] M. Tang, W. C. Carter, and R. M. Cannon. Diffuse interface model for structural transitions of grain boundaries. *Phys. Rev. B*, 73:024102, 2006.
- [19] Ryo Kobayashi and James A. Warren. Modeling the formation and dynamics of polycrystals in 3d. *Physica A*, 356:127–132, 2005.
- [20] G. Bortel T. Pusztai and L. Gránásy. Phase field theory of polycrystalline solidification in three dimensions. *EPL (Europhysics Letters)*, 71(1):131–137, 2005.
- [21] P.-G. de Gennes and J. Prost. *The physics of liquid crystals – second edition*. Clarendon Press, Oxford, UK, 1993.
- [22] R. Kobayashi and Y. Giga. Equations with singular diffusivity. *J. Stat. Phys.*, 95:1187–1220, 1999.
- [23] M. T. Lusk. A phase-field paradigm for grain growth and recrystallization. *Proc. R. Soc. London Ser. A-Math. Phys. Eng. Sci.*, 455(1982):677–700, 1999.
- [24] M. Rettenmayr. Melting and remelting phenomena. *Int. Mat. Rev.*, 54:1–17, 2009.
- [25] Saryu J. Fensin, David Olmsted, Dorel Buta, Mark Asta, Alain Karma, and J. J. Hoyt. Structural disjoining potential for grain-boundary premelting and grain coalescence from molecular-dynamics simulations. *Phys. Rev. E*, 81:031601, 2010.
- [26] T. Frolov and Y. Mishin. Liquid Nucleation at Superheated Grain Boundaries. *Phys. Rev. Lett.*, 106:155702, 2011.
- [27] Joel Berry, K. R. Elder, and Martin Grant. Melting at dislocations and grain boundaries: A phase field crystal study. *Phys. Rev. B*, 77:224114, 2008.
- [28] Jesper Mellenthin, Alain Karma, and Mathis Plapp. Phase-field crystal study of grain-boundary premelting. *PHYSICAL REVIEW B*, 78:184110, 2008.
- [29] M Rappaz, A Jacot, and WJ Boettinger. Last-stage solidification of alloys: Theoretical model of dendrite-arm and grain coalescence. *Met. Mat. Trans. A*, 34:467–479, 2003.
- [30] Y. Mishin, W. J. Boettinger, J. A. Warren, and G. B. McFadden. Thermodynamics of grain boundary premelting in alloys. I. Phase-field modeling. *Acta Mat.*, 57:3771–3785, 2009.
- [31] N. Wang, R. Spatschek, and A. Karma. Multi-phase-field analysis of short-range forces between diffuse interfaces. *Phys. Rev. E*, 81:051601, 2010.
- [32] H. Garcke, B. Nestler, and B. Stoth. On anisotropic order parameter models for multi-phase systems and their sharp interface limits. *Physica D*, 115:87–108, 1998.
- [33] M. Plapp. Remarks on some open problems in phase-field modelling of solidification. *Phil. Mag.*, 91:25–44, 2011.
- [34] A. Karma and W.-J. Rappel. Quantitative phase-field modeling of dendritic growth in two and three dimensions. *Phys Rev E*, 57:4323–4349, 1998.
- [35] Jesper Mellenthin. *Phase-field modelling of polycrystalline solidification*. Ph.d. thesis, Palaiseau, France, 2007.
- [36] A. Karma, D.A. Kessler, and H. Levine. Phase-field model of mode III dynamic fracture. *Phys. Rev. Lett.*, 87:045501, 2001.